Article

Spatial Resolution for X-ray Excited Luminescence Chemical Imaging (XELCI)

Apeksha C. Rajamanthrilage,[‡] Unaiza Uzair,[‡] Paul W. Millhouse, Matthew J. Case, Donald W. Benza, and Jeffrey N. Anker*

Cite This: *Chem. Biomed. Imaging* 2024, 2, 510–517

Read Online

ACCESS | Metrics & More | Article Recommendations | Supporting Information

ABSTRACT: Measuring chemical concentrations at the surface of implanted medical devices is important for elucidating the local biochemical environment, especially during implant infection. Although chemical indicator dyes enable chemical measurements in vitro, they are usually ineffective when measuring through tissue because the background obscures the dye signal and scattering dramatically reduces the spatial resolution. X-ray excited luminescent chemical imaging (XELCI) is a recent imaging modality which overcomes these limitations using a focused X-ray beam to excite a small spot of red light on scintillator-coated medical implants with well-defined location (because X-rays are minimally scattered) and low background. A spectrochemical indicator film placed over the scintillator layer, e.g., a polymer film containing pH-indicator dyes, absorbs some of the luminescence according to the local chemical environment, and this absorption is then detected by measuring the light intensity/spectrum passing through the tissue. A focused X-ray beam is used to scan point-by-point with a spatial resolution mainly limited by the X-ray beam width with minimum increase from X-ray absorption and scattering in the tissue. X-ray resolution, implant surface specificity, and chemical sensitivity are the three key features of XELCI. Here, we study spatial resolution using optically absorptive targets. For imaging a series of lines, the 20−80% knife-edge resolution was ∼285 (±15) μm with no tissue and 475 ± 18 and 520 ± 34 μm, respectively, through 5 and 10 mm thick tissue. Thus, doubling the tissue depth did not appreciably change the spatial resolution recorded through the tissue. This shows the promise of XELCI for submillimeter chemical imaging through tissue.
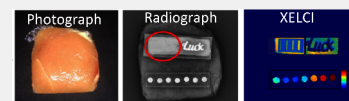
KEYWORDS: *Spatial resolution, Chemical imaging, X-ray imaging, Radioluminescence, pH imaging*

INTRODUCTION

Bacteria that colonize upon a medical implant can form biofilms which are highly resistant to antibiotics and the host's immune system.[1,2] Indeed, over one-half of hospital-acquired infections are associated with medical implants, and treatment often requires device removal with risks and costs,[3,4] especially once the biofilm has matured. The antibiotic and host resistance arises from multiple factors, including dormant regions with low pH, oxygen, and metabolic activity, poor penetration of antibiotics (dormant regions are especially likely to be inaccessible), and heterogeneous microenvironments with some regions in which antibiotics are less effective. Low pH can occur due to the biofilm and/or host inflammatory response, and this could potentially serve as both a local marker for infection and a potential for selective treatment of biofilms through either drugs that target low-pH regions or methods to raise the pH or increase metabolite and antibiotic transport to make biofilms more susceptible.[5] There is a need to develop techniques to measure biochemical concentrations at the surface of implanted medical devices for detecting infections, elucidating local physiology, and developing effective treatments. The sensor would need to sample the point of interest with high spatial resolution in order to study pH heterogeneity and be able to distinguish calibration references from sensor regions.

X-ray excited luminescent chemical imaging uses a focused X-ray beam to reach deep into the soft tissue without much scattering and produce a luminescent spot from an X-ray scintillator film coated on a medical implant.[6−10] The luminescence intensity is modulated by optical absorption from a chemical sensing film on the device. In principle, anything that absorbs light or alters the spectrum can be detected including pH indicators, silver/gold nanoparticles,[11] different types of phosphors,[12] and cut paper resolution targets used herein, and the approach can be generalized to a variety of spectrochemical and mechanical sensing techniques. After the luminescence passes through the sensor layer it then passes through tissue and is detected using a spectrometer or photomultiplier tubes (PMTs) coupled with optical filters. The technique is similar to X-ray luminescence tomography (XLT) except that XELCI produces a 2D image of the surface, while XLT generates 3D images of nanophosphor contrast agents.[13,14] It is also related to radioluminescence imaging
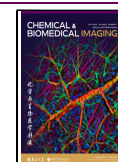
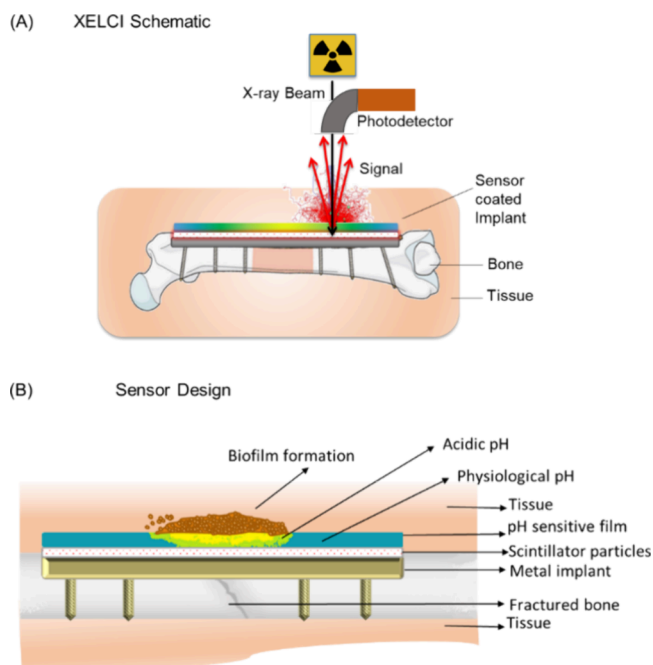except that an external X-ray beam is used to generate light in XELCI and detection is based on indicator dyes, as opposed to a lower resolution radionuclide-labeled drug for radio-luminescence imaging.[15] A schematic of the XELCI scanner is shown in Figure 1. The technique works in conjunction with

Figure 1. X-ray excited chemical luminescence imaging (XELCI). (A) Schematic of XELCI imaging. The sample is irradiated with a focused X-ray beam, and the resulting luminescent signal is collected with a photodetector. (B) Schematic of the sensor design. An orthopedic plate is coated with a scintillator layer that luminesces when excited by the X-ray. The scintillator layer is covered with a pH-sensitive layer that changes color depending on the surface pH and modulates the luminescence of the underlying layer, indicating pH.

a sensor that is coated on the surface of the implanted device, the design of which is given in Figure 1B. The pH sensor on the implant consists of two layers: the bottom layer contains Gd_2O_2S:Eu scintillator microphosphors in polydimethylsiloxane (PDMS) which emit 620 and 700 nm when irradiated with an X-ray. This scintillator layer is covered by a pH-indicating hydrogel layer that changes color according to pH such that in basic pH more of the 620 nm light from the scintillator is absorbed compared to in acidic pH. Thus, the pH-indictor layer modulates the luminescent signal from the scintillator layer and allows for the mapping of surface pH. The 700 nm scintillator emission remains unaltered as it is not absorbed by the pH layer and thus serves as an in situ spectral reference to account for pH-independent attenuation of the luminescent signal by tissue and variable optical collection efficiency.

By coating the surface of the medical implants with the pH-indicator layers, we can use XELCI to image the pH changes associated with implant-associated infections such as those commonly observed with orthopedic implants. Figure 1B shows an orthopedic plate coated with the sensor layers, and the pH layer is changing color (turning yellow) in areas of biofilm growth, indicating infection. This color change that is otherwise impossible to see with the naked eye or even with plain X-ray images can be visualized using XELCI.

pH can be measured in many ways. Yuqing et al. provided a review of different technologies being developed for pH sensing including pH sensors based on optical fibers, mass-sensitive hydrogels, metal−oxides, conducting polymers, nano-constructed cantilevers, and the magnetoelastic effect.[16] Implantable pH sensors are promising, but active sensors need to overcome issues of power, telemetry, drift, and biofouling. Wireless pH sensors, such as the one based on a carbon nanotube chemiresistor coupled with an RFID tag, can provide remote wireless chemical sensing, but a major limitation would be continuous coating of the implant surface with the chemiresistor and RFID tags.[17] Electrochemical sensors are notorious for biofouling when implanted in vivo due to adsorption of the proteins on the sensor surface, hence causing a drift in the measurements of the electric current or voltage, a nonequilibrium process (at equilibrium, the voltage and current would be 0).[18] Optical sensors, on the other hand, measure the equilibrium response of a pH dye that does not suffer from drift unless the microenvironment changes. Passive sensors such as those based on XELCI, radiographic sensors, and optical sensors perform better in vivo as their sensing mechanisms are less susceptible to be affected by biofouling, do not require complex circuitry, and can be easily adapted to different types of implants.

Computed tomography (CT) and magnetic resonance imaging (MRI) provide information on the extent of bone necrosis and soft tissue abnormalities but do have the disadvantage of imaging interferences in the vicinity of metal implants. Nuclear imaging techniques such as [^{18}F]-fluorodeoxyglucose positron emission tomography (FDG-18 PET) or technetium-99m uptake imaging provide important information on the local metabolic activity which may aid in diagnosing implant-associated osteomyelitis, though such imaging is expensive, relies on systemic absorption of radioactive material, and yields no information on the local pH of the region.[19] None of these methods provide sufficient means for early detection of implant-associated infection which can be helpful for successful treatment of infection without the need to remove the implant and avoid extra medical and surgical expenses. It is also important to monitor the course of infection during treatment to evaluate the success of treatment. After an antibiotic therapy, there is a good chance for the surviving bacteria to slowly re-establish a biofilm,[20] which creates a need for periodic monitoring of implant infection during and after treatment. These imaging techniques can be used in parallel with our approach to confirm clinical findings.

Figure 2A shows the three key features of XELCI and compares it with other imaging techniques in terms of imaging resolution and tissue depth (Figure 2B). Optical microscopy is highlighted for ballistically propagating optical photons (including diffraction-limited fluorescence confocal micros-copy and superresolution techniques such as stimulated emission depletion (STED) and photoactivated localization microscopy (PALM)). For imaging beyond ~1 mm of tissue, where few ballistic photons penetrated, medical imaging techniques dominate. XELCI sits next to photoacoustic tomography (PAT), single-photon emission computed tomog-raphy (SPECT), positron emission tomography (PET), ultrasound (US), X-ray computed tomography (CT), and magnetic resonance imaging (MRI) and can image through deep tissue at least up to 2 cm thick with high resolution. In addition to deep tissue imaging, XELCI provides chemical sensitivity and surface-specific information such as localized
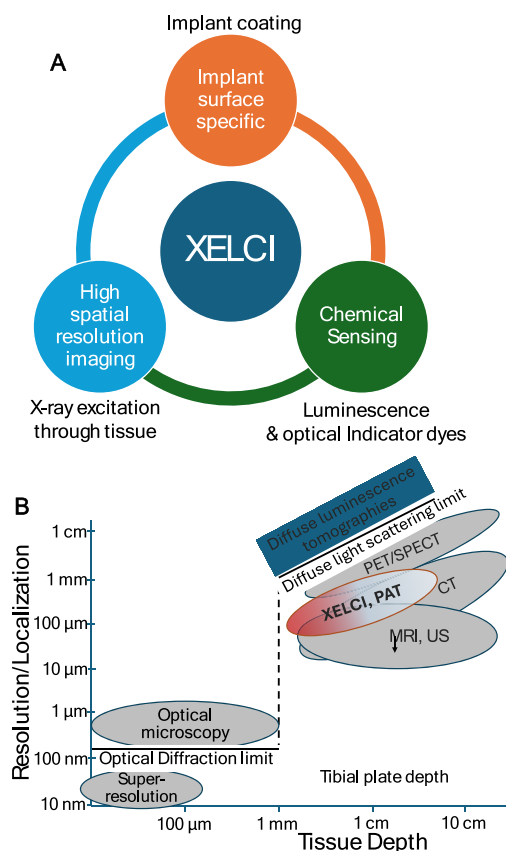
Figure 2. Advantages of XELCI and comparison with other imaging modalities. (A) Diagram highlighting three key features of XELCI. (B) Image resolution and depth for various modalities. Microscopy techniques for ballistically propagating optical photons <∼1 mm are clearly distinguished from medical imaging techniques through from 1 mm to 10 cm of tissue. XELCI and photoacoustic tomography (PAT), highlighted in red, have advantages for imaging through several millimeters to ∼3 cm of tissue.

pH changes that are specific to the surface of medical implants. Our approach is innovative because no other medical imaging technique measures surface-specific chemical concentrations at high resolution through thick tissue. Other techniques (e.g., MRI, plain X-ray, CT, US, and PET) lack surface-specific pH contrast agents, and optical tomography techniques have poor lateral resolution through tissue (>1 mm thick because tissue scatters and prevents the incident optical beam from focusing).

That said, each technique has its advantages, and combining multiple image modalities can provide complementary anatomical and contrast-related information. Fortunately, XELCI uses solid implants which will show up on the other imaging techniques, simplifying coregistration; X-ray imaging is especially easy since the XELCI setup already has an X-ray source.[6,7,10]

■ METHODS

XELCI Scanner Setup

In the XELCI scanner setup, Figure 3, the X-ray is positioned from the top directly perpendicular to the sample stage. For light to propagate through a light guide, it must enter at an angle less than the maximum acceptance angle to the axis of the light guide. Any light entering the light guide at an angle greater than the acceptance angle will not be able to propagate through and will be lost. By using a light guide with a large acceptance angle, we can dramatically increase the signal collection by collecting light from more angles after it is being scattered through the tissue. Acrylic (poly(methyl methacrylate)) in air essentially accepts everything with a theoretical maximum acceptance angle of 90°.

In addition to offering the advantage of collecting more light with a greater acceptance angle, the acrylic light guide can be placed almost in close contact with tissue and increase the core diameter of the acrylic rod to collect light from a larger area. It can also be aligned with the X-ray beam in a straight line by having an alignment hole in the elbow-shaped mirror attachment that collects and reflects the signal into the acrylic rod.

X-ray Beam Width Measurements

A radiochromic film (Gafchromic EBT3-1417, Lot # 09241801, Ashland Global Specialty Chemicals Inc., DE, USA) was roughly cut into small rectangular pieces and placed at 5 mm intervals in a 3D-printed holder that had 15 slots 5 mm apart. The holder with pieces of the radiochromic film was placed vertically under the X-ray beam with the radiochromic piece in the 0 mm slot directly in contact with the focusing optics (polycapillary) of the X-ray and exposed to the X-ray beam (at 50 kV and 600 μA) for 30 s. The spot size was measured with ImageJ software.

Luminescence Point Spread Function through Tissue

To visualize the light transmittance of a point source through tissue, a scintillator film was made with a 1:1 mass ratio of gadolinium oxysulfide doped with europium ($Gd_2O_2S:Eu$) phosphors (Phosphor Technologies Ltd., UK) in polydimethylsiloxane (PDMS). The film was placed under the focused X-ray beam (iMOXS, Institute for Scientific Instruments GmbH, Berlin, Germany) at 5 cm from the tip of the focusing optics (focal distance of the X-ray focusing optics) and photographed in the dark with the X-ray on. We see the red
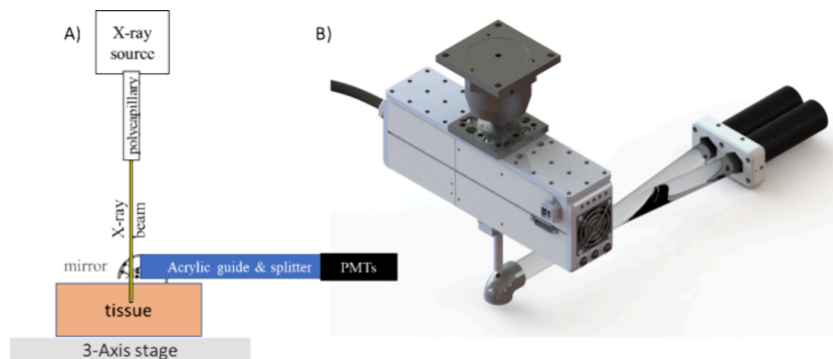
Figure 3. Optimized XELCI setup. (A) Schematic of the optimized XELCI system with a horizontal acrylic light guide for signal collection. Note, the tissue specimen is on a 3-axis stage to move the sample beneath the beam. (B) Solidworks 3D rendering of the setup showing the X-ray source, mirror, lightguide/splitter, and 2 PMTs.

luminescence spot generated by the X-ray beam irradiation of the scintillator film in Figure 4. The scintillator film was then covered with
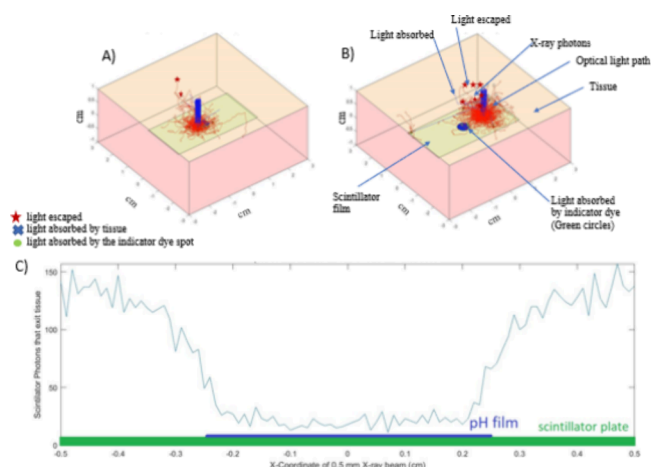
Figure 4. Simulated XELCI imaging of a 5 mm pH-sensitive dye spot on a scintillator through 1 cm thick tissue. (A) Simulation with the X-ray beam just over the dye spot. (B) Simulation with the X-ray beam just past the dye spot. (C) Line profile showing the number of photons that escaped through tissue vs X-ray beam position.

5 and 10 mm (±1 mm) thick pieces of chicken breast (cut into slices using an electric food slicer (model 630, Chef's Choice, Avondale, PA, USA)) and photographed again. The spot sizes were measured at each occasion.

Knife-Edge Resolution Experiment

A line target with four different line widths was laser cut from a piece of black cardboard. The line target contains 4 different line widths: 2, 1, 0.5, and 0.2 mm. It was placed over a scintillator layer as shown in Figure 5A. XELCI imaging of the line target was carried out through 0, 5, and 10 mm porcine tissue. The 620 nm images are shown in Figure 5B−D.

XELCI vs Plain Radiography

A line target, pH discs at different pHs (pH 6.5 and 7.5), and a metal target (Luck sign) were used to compare the functional radiography
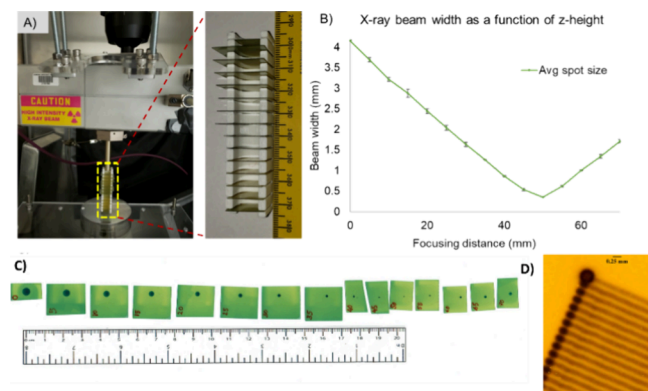
Figure 5. Determination of the X-ray beam width at different heights. (A) Photograph of the experimental setup. Pieces of radiochromic film were lined up at different heights in a 3D-printed holder and placed under the X-ray focusing optics. (B) Plot of the spot size generated by the X-ray beam at different heights. (C) Photograph of the spot sizes generated by the focused X-ray beam at different angles. (D) The beam is not uniform and a faster scan (5 mm/s) shows ~0.1 mm line width when moving with a larger spot when paused at end of the line.

technique, XELCI with plain radiography. The line target was made by laser cutting a piece of black paper with four different line widths: 2, 1, 0.5, and 0.2 mm. All three targets were placed on a scintillator layer as shown in Figure 3A. These were first imaged with plain radiography and then with XELCI. The three targets on the scintillator layer were then covered with porcine tissue and imaged again with plain radiography and XELCI.

Light Propagation Simulations

Monte Carlo simulations were performed, where a collimated X-ray photon was randomly chosen within a 0.25 mm diameter beam. It then propagated through 1 cm of tissue; at each step, the photon is either absorbed (with a probability defined by the X-ray tissue absorption coefficient from the NIST standard reference database 126 on X-ray Mass Attenuation Coefficients), scattered (with a probability from the same NIST standard reference database with an angular scattering distribution defined by the Klien−Nishina equation), or if not absorbed or scattered moves forward ballistically. The photon's position and direction are recorded at each step. If it reaches the scintillator, it is assumed to be absorbed and converted to visible light (a more sophisticated model would include the energy absorption coefficient in the Gd_2O_2S film, but this is relatively high: Gd_2O_2S has a penetration depth of around 40 μm for 20 keV photons). The visible light is then propagated back through the pH-indicator film and then through the tissue. Visible photons are absorbed or scattered according to the tissue's characteristics ($\mu_s = 1/100$ μm; $g = \langle \cos(\theta) \rangle$ = 0.95; $\mu_a = 1/1.7$ cm). If incident on the scintillator, they are assumed to pass through the film again and reflect back. The number of photons reaching/passing through the top of the tissue slab are then counted to estimate line profiles.

■ RESULTS AND DISCUSSION

To see how the XELCI spatial resolution compared with the X-ray beam width and optical spatial resolution, we measured the X-ray beam width, the point spread function through tissue, and the XELCI knife-edge resolution and compared them with simulations. Fundamentally, we expect approximately exponential attenuation of X-ray and optical signals (with photon energy/wavelength-dependent spectral distortion). The X-rays with a mean free scattering path length of 1−10 cm (depending on the photon energy) should maintain focus through the tissue with some background from the scattered X-rays, while the visible light with a mean free scattering path of ~100 μm through the tissue and a scattering anisotropy factor of 0.8−0.95 essentially travel diffusively through the tissue, exiting the top of the tissue as a blurred spot with a full width-half-max around the depth of the tissue being imaged. The collection optic has a 1 in. diameter and can collect most of the emitted light, but the resolution of the XELCI should be much better, limited by the X-ray beam width used to excite the scintillators (with some spread from optical scattering in the scintillator film).

■ MONTE CARLO PHOTON PROPAGATION SIMULATION

We ran Monte Carlo simulations in MATLAB to illustrate how XELCI functions considering the light interactions (photon scattering and absorption) with tissue. Light scattering and absorption are wavelength-dependent events, and X-rays have very low scattering and absorption coefficients compared to visible light. Thus, as shown in Figure 4A and 4B, the X-rays (blue) penetrate deeply through the tissue with minimal scattering and absorption. A scintillator film with a centered blue spot (pH-sensitive dye) is located in the tissue. To imitate the XELCI imaging system, an X-ray beam is scanned over the scintillator film and generates red photons. These photons can

escape the tissue, scatter, be absorbed in the tissue, or be absorbed by the pH dye close to the surface of the scintillator film. When the X-ray beam is focused near the dye spot, many of the generated visible photons are absorbed by the dye, so fewer visible photons pass through the tissue and are detected.

Essentially all of the visible light exiting the tissue has experienced multiple scattering events and has a relatively large width (point spread function). However, the integrated signal depends very strongly upon the local absorption from the pH sensor film near the incident X-ray beam, and the resulting XELCI image has a width limited by the X-ray beam width. For example, Figure 4 simulates an XELCI image of a 5 mm circular region that strongly absorbs light measured through 1 cm of tissue; this simulated XELCI image has a line profile which changes over just 1.5 mm, an order of magnitude less than the point spread function. This depends upon the X-ray beam width.

◼ X-RAY BEAM WIDTH MEASUREMENTS

The X-ray source is fitted with a polycapillary that focus the X-ray beam to a fine spot. Since XELCI resolution is limited by the X-ray excitation beam, we characterized the spot size of the X-ray beam as a function of height to find the optimum distance where the X-ray beam is best focused. A radiochromic film (Gafchromic) was used to visualize the X-ray beam spot. Radiochromic films are self-developing films containing a dye that changes color when exposed to ionizing radiation, thus allowing the level of exposure and beam profile to be characterized. Figure 5A shows the experimental setup where the radiochromic films are lined up under the X-ray beam at 5 mm intervals starting at a height of 0 mm from the polycapillary to 7 cm below it. The radiochromic films were exposed simultaneously for 30 s to an X-ray beam of 50 kV and 600 μA (same as used for XELCI imaging). The spot size is plotted as a function of height in Figure 5B, and a photograph of the radiochromic films after exposure visualizing the X-ray beam spot is shown in Figure 5C. The X-ray beam has a width of 4.16 mm when it exits the polycapillary at 0 mm that gradually decreases and is focused to a fine spot of 0.36 mm at a vertical distance of 5 cm from the polycapillary. The beam width starts increasing again after 5 cm. Therefore, 5 cm is the optimum imaging distance between the sample and the X-ray polycapillary to make sure the X-ray beam is properly focused. This agrees with the spot size (0.38 mm) calculated using the full width at half-maximum (fwhm) of the red-light intensity spot generated on the scintillator film when irradiated by a focused X-ray beam 5 cm from the end of the polycapillary (Figure 6). However, we expect the actual X-ray beam width to be smaller than the spot size generated on the scintillator film as the thickness of the scintillator film can also diffuse the light generated by the X-ray beam. XELCI collects the signal generated from point-by-point excitation of the scintillator film with the X-ray beam, and the width of the X-ray beam is the key factor in determining the spatial resolution.

The intensity of the X-ray beam at the focusing height (5 cm) or tissue surface was also determined by comparing the radiochromic film with the exposure calibration reference of the same film provided by the manufacturer. At a scan speed of 5 mm/s with a step size of 250 μm, the maximum local absorbed dose was found to be 50 rad or 0.5 Gy; and the total local depends on the scanning speed, step size, and duration of the scan. This is below the limit for causing cutaneous radiation injury, also known as radiation burns that can occur
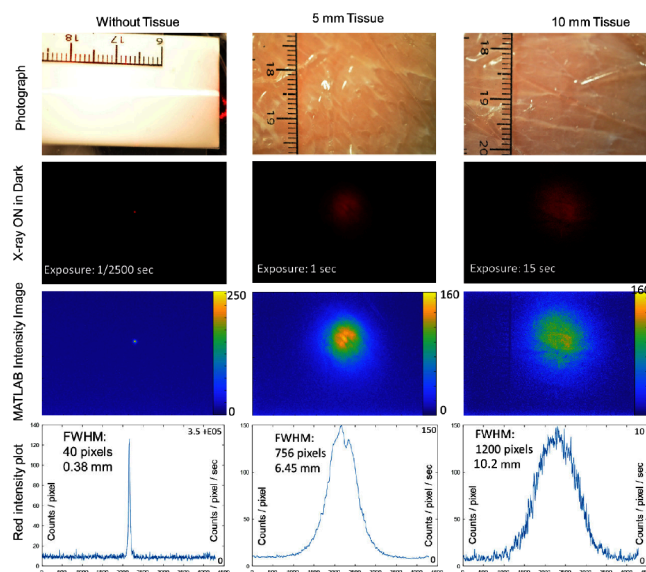
Figure 6. Point spread function (scintillator film irradiated with a focused X-ray beam). Photograph of the scintillator film without any covering and covered with 5 mm and 1 cm thick slices of chicken breast tissue. The scintillator film was irradiated with a focused X-ray beam to generate red light and imaged with a digital camera in the dark with and without the tissue coverings. Images were analyzed using MATLAB and red-light intensity (counts/pixel) plotted to calculate the point spread function of the irradiated spot without and through tissue.

from a radiation dose as low as 2 Gy.[21] The 0.5 Gy dose represents the localized dose absorbed at the skin with no filters in the X-ray beam and will be much lower either with a filter or within the muscle tissue underneath the skin as we are using a relatively lower energy X-ray beam (50 kV tungsten source with a polycapillary that works below ∼30 keV). The long-term stochastic risks association with such irradiation can be better estimated by converting this localized absorbed dose to an average full body effective dose. Assuming the imaging area to be 1 cm^2 and that all X-ray energy is absorbed before or within the implant, which is 1 cm deep, we get an exposed mass of about 1 g of tissue (somewhat less if we discount X-ray energy absorbed by the implant). For a 5 kg rabbit and conservatively weighting all tissue evenly, this would correspond to an average full body dose of 0.1 mSv. This is typical of a chest X-ray exam that is about 70× less than that of a chest CT scan (7 mSv). Standard radiographic exams range from 0.01 to 10 mSv, while CT scans can have an effective radiation dose of 2−20 mSv.[22]

### ◼ LINE SPREAD FUNCTION THROUGH TISSUE

To visualize how the light from our scintillator spreads as it propagates through tissue and observe the point spread function, we placed the Gd_2O_2S:Eu film at the X-ray focal distance and photographed the luminescence through varying tissue thicknesses either with room light on or in the dark with the X-ray on (Figure 6). We then analyzed the red channel in MATLAB and measured the full width at half-maximum intensity to estimate the spread. Without any tissue, a bright spot is observed with a fwhm of ∼380 μm. The scintillator film was then covered with 5 and 10 mm (±1 mm) thick pieces of chicken tissue and photographed again. We can see the spot size (fwhm) increased to about 6.5 and 10.2 mm after passing

through 5 mm and 1 cm thick chicken tissue, respectively. This is consistent with theory and previous studies which have shown that the point spread function is typically similar to but somewhat larger than the depth of the tissue being imaged through, with the precise calculation dependent on the sample and samples/wavelengths with a larger absorption coefficient attenuating longer pathlengths and reducing the radial spread at the skin surface (smaller point spread function).[23]

The spot is not uniform after passing through tissue, especially through 5 mm thick tissue, indicating that the tissue absorption, scattering, and/or thickness is somewhat inhomogeneous. This sample-, wavelength-, and position-dependent point spread function makes it very difficult to deconvolve luminescence images based on a simple point spread function estimate (noise also hampers such reconstruction). In addition to the increasing radius and changing shape of the spot after the light after passes through the tissue (Figure 6), the absolute intensity also decreases. We increased the exposure with increasing tissue thickness so that we would have enough signal to measure and compare from 1/2500 s with no tissue to 15 s through 10 mm of tissue. Thus, while the y-axis counts/pixel is almost constant, the power/pixel decreases significantly (second y axis). Integrating over the luminescence spot area, the overall signal decreases by a factor of around 50.

## ■ KNIFE-EDGE RESOLUTION EXPERIMENT

Since the X-ray beam penetrates deeply through tissue with minimal scattering in the tissue, we expect XELCI to have high spatial resolution for imaging local absorption on the film. The spatial resolution is mainly expected to be limited by the width of the X-ray beam with some additional broadening from light scattering and propagation within the scintillator and indicator or target films and potentially some effect from backscatter in thick tissue. A line target was prepared by laser cutting lines of defined width in a black paper (optically absorbing, 100 μm thick) and imaged with XELCI through tissue and without any tissue covering. The lines had a width of 2, 1, 0.5, and 0.2 mm. A photograph of the line target placed on the scintillator film and the 620 nm intensity XELCI images of the target scanned with and without tissue (5 and 10 mm thick tissue) are shown in Figure 7 along with the intensity plots. We can clearly see all of the lines in the XELCI images both with and without tissue. The signal is plotted as an intensity plot for the line drawn across the XELCI images in Figure 7b, 7e, and 7h. The areas containing the cut-out lines in the paper allowed transmittance of the optical signal as indicated by the peaks, and the area that was covered with black paper did not allow the signal to pass (valleys in the intensity plot). To determine the knife-edge resolution for 20−80% intensity transition, the falling edge of the 2 mm line peak was selected (zoomed in, Figure 7c, 7f, and 7i). The 20−80% intensity transition occurred over 285 ± 14 μm with no tissue, 475 ± 18 μm through 5 mm tissue, and 520 ± 34 μm through 10 mm tissue. The spatial resolution should not significantly vary with or without tissue due to the minimal X-ray scattering through 5 mm of tissue by the X-ray beam. Additionally observed slight differences may be due to positioning of the target as it appears to be the case in the XELCI image where the target might not be completely flat on the scintillator film.
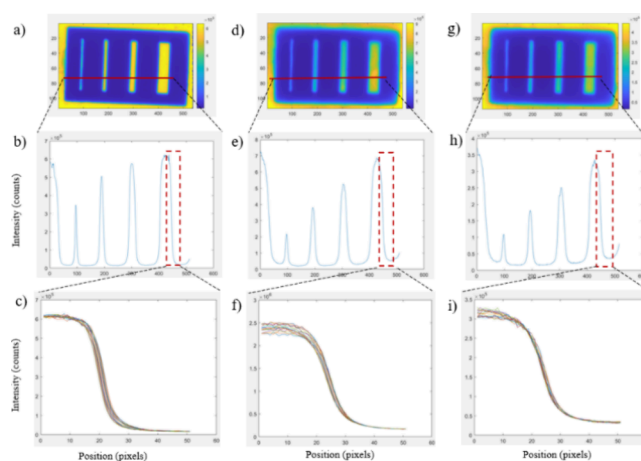
Figure 7. XELCI Images of the line target and graphs showing 700 nm light intensity changes across the lines and light changes with position at the edge of the 2 mm wide line. (a) XELCI intensity image of 700 nm light through no tissue. (b) Corresponding line profiles across the four line widths with no tissue. (c) Line profile zoom in at the edge of the 2 mm wide line with no tissue. (d) XELCI intensity image of 700 nm light through 5 mm tissue. (e) Corresponding line profiles across the four line widths through 5 mm tissue. (f) Line profile zoom in at the edge of the 2 mm wide line through 5 mm tissue. (g) XELCI intensity image of 700 nm light through 10 mm tissue. (h) Corresponding line profile across the four line widths through 10 mm tissue. (i) Line profile zoom in with position at the edge of the 2 mm wide line through 10 mm tissue. Each pixel is 40 μm.

■ XELCI VS PLAIN RADIOGRAPHY

XELCI can be categorized as functional radiography providing chemical sensitivity coupled with the penetration depth of plain radiography. Figure 8 shows a side-by-side comparison of
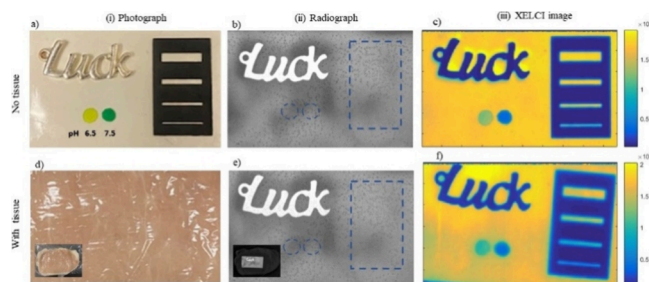
Figure 8. Comparison of plain radiography vs XELCI imaging. (a) Photograph of the three targets (metal "Luck" target, pH sensitive hydrogel at two different pHs, line target with different line widths) on the scintillator film with no tissue. (b) Radiograph of the three targets with no tissue. (c) XELCI image of the three targets with no tissue. (d) Photograph of the three targets on the scintillator film with 5 mm tissue. (e) Radiograph of the three targets with tissue. (f) XELCI image of the three targets with 5 mm tissue.

XELCI with plain radiography. There are three targets in the figure: (1) Different line widths cut out in a black paper that blocks visible light, (2) a radio-opaque metal target (Luck sign), and (3) two discs of gel at different pHs (6.5, 7.5). All three targets were placed on a scintillator layer. Images of these targets were acquired using a digital camera, X-ray radiograph, and XELCI first without any tissue and later covered with a piece of 1 cm thick porcine tissue. When the targets were covered with tissue, they could not be observed via

photography and only the tissue surface of the tissue was evident. X-ray radiography shows the metal keychain, the scintillator film, and the tissue slice. However, the paper target and pH-indicator gel discs cannot be observed because they do not attenuate X-rays. By contrast, the XELCI images with and without tissue clearly show the three targets and provide chemical sensitivity with regard to the pH of the discs. The XELCI images provide high spatial resolution as we can see the lines in the paper target and clearly read the letters of the metal target. The width of the lines in the paper target were 2, 1, 0.5, and 0.2 mm (top to bottom). Supporting Information Figure SI 1 shows XELCI images of 7 scintillator discs with pH-indicator films placed over them and exposed to different pHs (as well as the other two targets). This shows small films can be made and implanted separately; the XELCI image is also a composite from three regions of interest to speed up acquisition.

■ CONCLUSION

X-ray excited luminescent chemical imaging (XELCI) is a technique to map chemical concentrations on the surface of medical devices embedded in tissue. It combines the spatial resolution of X-ray with surface-specific chemical sensitivity for deep tissue imaging. The system was characterized in terms of X-ray beam width and spatial resolution. The X-ray beam could be focused to a 0.36 mm fine spot for point-by-point excitation of the sample. The spatial resolution of the XELCI images through tissue is limited primarily by the width of the X-ray beam and was determined to be about 500 μm. The point spread function of light from a point source passing through tissue was characterized, and the XELCI system was optimized to collect more signal by increasing the core diameter and the acceptance angle of the signal-collecting light guide. These features are important for explaining how XELCI can noninvasively measure optical absorption on the surface of implanted medical devices, including for pH imaging during implant infection. Future work includes applying XELCI to in vivo imaging of pH and other analytes in bones and tissue with superimposed X-ray imaging of anatomy.

■ ASSOCIATED CONTENT

Ⓢⓘ Supporting Information

The Supporting Information is available free of charge at https://pubs.acs.org/doi/10.1021/cbmi.4c00039.

> Additional photograph, radiograph, and XELCI images of the target with and without tissue at several pHs (PDF)

■ AUTHOR INFORMATION

Corresponding Author

Jeffrey N. Anker − *Department of Chemistry, Clemson University, Clemson, South Carolina 29634, United States;* ⓞ orcid.org/0000-0002-9544-2367; Email: janker@clemson.edu

Authors

Apeksha C. Rajamanthrilage − *Department of Chemistry, Clemson University, Clemson, South Carolina 29634, United States;* Present Address: Sonder Research X, North Brunswick, New Jersey 08902, United States

Unaiza Uzair − *Department of Chemistry, Clemson University, Clemson, South Carolina 29634, United States;* Present Address: Chemical and Biomolecular Analysis Facility, Augusta University, Augusta, Georgia 30912, United States.; ⓞ orcid.org/0000-0002-8249-8791

Paul W. Millhouse − *Department of Chemistry, Clemson University, Clemson, South Carolina 29634, United States;* Present Address: PM&R at Thomas Jefferson University Hospital, Philadelphia, Pennsylvania 19107, United States.

Matthew J. Case − *Department of Chemistry, Clemson University, Clemson, South Carolina 29634, United States;* Present Address: Department of Radiation Oncology, Emory University, Atlanta, Georgia 30322, United States.

Donald W. Benza − *Department of Chemistry, Clemson University, Clemson, South Carolina 29634, United States;* Present Address: Savannah River National Lab, Aitken, South Carolina 29808, United States.

Complete contact information is available at:
https://pubs.acs.org/10.1021/cbmi.4c00039

Author Contributions

[‡]A.C.R. and U.U.: These authors contributed equally. The manuscript was written through contributions of all authors. All authors have given approval to the final version of the manuscript.

Notes

The authors declare no competing financial interest.

■ ABBREVIATIONS

CT, computed tomography; fwhm, full width at half-maximum; PALM, photoactivated localization microscopy; PAT:, photoacoustic tomography; PET, positron emission tomography; PMT, photomultiplier tube; SPECT, single-photon emission computed tomography; STED, stimulated emission depletion; US, ultrasound; XELCI, X-ray luminescence chemical imaging; XLT, X-ray luminescence tomography

■ REFERENCES

(1) Gimeno, M.; Pinczowski, P.; Pérez, M.; Giorello, A.; Martínez, M. Á.; Santamaría, J.; Arruebo, M.; Luján, L. A Controlled Antibiotic Release System to Prevent Orthopedic-Implant Associated Infections: An in Vitro Study. *Eur. J. Pharm. Biopharm.* **2015**, *96*, 264−271.

(2) Kirby, J. P.; Mazuski, J. E. Prevention of Surgical Site Infection. *Surg. Clin. North Am.* **2009**, *89* (2), 365−389.

(3) Bryers, J. D. Medical Biofilms. *Biotechnol. Bioeng.* **2008**, *100* (1), 1−18.

(4) Vertes, A.; Hitchins, V.; Phillips, K. S. Analytical Challenges of Microbial Biofilms on Medical Devices. *Anal. Chem.* **2012**, *84* (9), 3858−3866.

(5) Behbahani, S. B.; Kiridena, S. D.; Wijayaratna, U. N.; Taylor, C.; Anker, J. N.; Tzeng, T.-R. J. pH Variation in Medical Implant Biofilms: Causes, Measurements, and Its Implications for Antibiotic Resistance. *Front. Microbiol.* **2022**, *13*, 4014.

(6) Uzair, U.; Benza, D.; Behrend, C. J.; Anker, J. N. Noninvasively Imaging pH at the Surface of Implanted Orthopedic Devices with X-Ray Excited Luminescence Chemical Imaging. *ACS Sens.* **2019**, *4* (9), 2367−2374.

(7) Uzair, U. A pH Sensor for Non-Invasive Detection and Monitoring of pH Changes During Implant-Associated Infection

Using X-Ray Excited Luminescence Chemical Imaging. *Ph.D. Dissertation*, Clemson University: Clemson, SC, 2020; DOI: 10.5555/AAI27838346; https://tigerprints.clemson.edu/all_dissertations/2655.

(8) Wang, F.; Raval, Y.; Tzeng, T. J.; Anker, J. N. X-Ray Excited Luminescence Chemical Imaging of Bacterial Growth on Surfaces Implanted in Tissue. *Adv. Healthc. Mater.* **2015**, *4* (6), 903−910.

(9) Chen, H.; Rogalski, M. M.; Anker, J. N. Advances in Functional X-Ray Imaging Techniques and Contrast Agents. *Phys. Chem. Chem. Phys.* **2012**, *14* (39), 13469.

(10) Rajamanthrilage, A. C.; Levon, E.; Uzair, U.; Taylor, C.; Tzeng, T.-R.; Anker, J. N. High Spatial Resolution Chemical Imaging of Implant-Associated Infections with X-Ray Excited Luminescence Chemical Imaging Through Tissue. *J. Vis. Exp.* , **2022**, No. 187, e64252.

(11) Chen, H.; Longfield, D. E.; Varahagiri, V. S.; Nguyen, K. T.; Patrick, A. L.; Qian, H.; VanDerveer, D. G.; Anker, J. N. Optical Imaging in Tissue with X-Ray Excited Luminescent Sensors. *Analyst* **2011**, *136* (17), 3438−3445.

(12) Chen, H.; Patrick, A. L.; Yang, Z.; VanDerveer, D. G.; Anker, J. N. High-Resolution Chemical Imaging through Tissue with an X-Ray Scintillator Sensor. *Anal. Chem.* **2011**, *83* (13), 5045−5049.

(13) Pratx, G.; Carpenter, C. M.; Sun, C.; Xing, L. X-Ray Luminescence Computed Tomography via Selective Excitation: A Feasibility Study. *IEEE Trans. Med. Imaging* **2010**, *29* (12), 1992−1999.

(14) Zhang, W.; Lun, M. C.; Nguyen, A. A.-T.; Li, C. X-Ray Luminescence Computed Tomography Using a Focused x-Ray Beam. *J. Biomed. Opt.* **2017**, *22* (11), 116004.

(15) Schober, G. B.; Anker, J. N. Radioluminescence Imaging of Drug Elution from Biomedical Implants. *Adv. Funct. Mater.* **2022**, *32* (2), 2106508.

(16) Yuqing, M.; Jianrong, C.; Keming, F. New Technology for the Detection of pH. *J. Biochem. Biophys. Methods* **2005**, *63* (1), 1−9.

(17) Gou, P.; Kraut, N. D.; Feigel, I. M.; Bai, H.; Morgan, G. J.; Chen, Y.; Tang, Y.; Bocan, K.; Stachel, J.; Berger, L.; Mickle, M.; Sejdić, E.; Star, A. Carbon Nanotube Chemiresistor for Wireless pH Sensing. *Sci. Rep.* **2014**, *4* (1), 4468.

(18) Frost, M. C.; Meyerhoff, M. E. Implantable Chemical Sensors for Real-Time Clinical Monitoring: Progress and Challenges. *Curr. Opin. Chem. Biol.* **2002**, *6* (5), 633−641.

(19) Trampuz, A.; Zimmerli, W. Diagnosis and Treatment of Infections Associated with Fracture-Fixation Devices. *Injury* **2006**, *37* (2), S59−66.

(20) Broekhuizen, C. a. N.; Sta, M.; Vandenbroucke-Grauls, C. M. J. E.; Zaat, S. a. J. Microscopic Detection of Viable Staphylococcus Epidermidis in Peri-Implant Tissue in Experimental Biomaterial-Associated Infection, Identified by Bromodeoxyuridine Incorporation. *Infect. Immun.* **2010**, *78* (3), 954−962.

(21) Wagner, L. Radiation Injury Is a Potentially Serious Complication to Fluoroscopically-Guided Complex Interventions. *Biomed. Imaging Interv. J.* **2007**, *3* (2), e22.

(22) Mettler, F. A.; Huda, W.; Yoshizumi, T. T.; Mahesh, M. Effective Doses in Radiology and Diagnostic Nuclear Medicine: A Catalog. *Radiology* **2008**, *248* (1), 254−263.

(23) Shimizu, K.; Tochio, K.; Kato, Y. Improvement of transcutaneous fluorescent images with a depth-dependent point-spread function. *Appl. Opt.* **2005**, *44* (11), 2154−2161.